



**HAL**  
open science

## Unrecognized pollution by inorganic condensable particulate matter in the atmosphere

Mengying Li, Shaocai Yu, Pengfei Li, Xue Chen, Zhe Song, Weiping Liu,  
Xiaoye Zhang, Meigen Zhang, Yele Sun, Zirui Liu, et al.

► **To cite this version:**

Mengying Li, Shaocai Yu, Pengfei Li, Xue Chen, Zhe Song, et al.. Unrecognized pollution by inorganic condensable particulate matter in the atmosphere. *Environmental Chemistry Letters*, 2024, 22, pp.49 - 56. 10.1007/s10311-023-01644-9 . hal-04420968

**HAL Id: hal-04420968**

**<https://hal.science/hal-04420968>**

Submitted on 27 Jan 2024

**HAL** is a multi-disciplinary open access archive for the deposit and dissemination of scientific research documents, whether they are published or not. The documents may come from teaching and research institutions in France or abroad, or from public or private research centers.

L'archive ouverte pluridisciplinaire **HAL**, est destinée au dépôt et à la diffusion de documents scientifiques de niveau recherche, publiés ou non, émanant des établissements d'enseignement et de recherche français ou étrangers, des laboratoires publics ou privés.

# Unrecognized pollution by inorganic condensable particulate matter in the atmosphere

Mengying Li<sup>1,12</sup> · Shaocai Yu<sup>1</sup>  · Pengfei Li<sup>2</sup> · Xue Chen<sup>1</sup> · Zhe Song<sup>1</sup> · Weiping Liu<sup>1</sup> · Xiaoye Zhang<sup>1,3</sup> · Meigen Zhang<sup>4,5,6</sup> · Yele Sun<sup>4,5</sup> · Zirui Liu<sup>4</sup> · Jingkun Jiang<sup>7,8</sup> · Eric Lichtfouse<sup>9</sup>  · Daniel Rosenfeld<sup>10</sup> · John H. Seinfeld<sup>11</sup>

## Abstract

Protecting the population from aerosol pollution relies on forecasts using models with aerosol composition, yet the respective contributions of aerosol components are poorly known. In particular, the contribution of inorganic condensable particulate matter (PM) to aerosols is likely to be underestimated in most models because condensable particulate matter exceeds the amount of filterable particulate matter in emissions from stationary combustion sources. Moreover, condensable particulate matter is rarely included in current emission inventories. Here, we estimated the emissions of inorganic condensable particulate matter from stationary combustion sources based on monitoring information in China. Then we modeled the contributions of condensable particulate matter to simulated inorganic aerosols, e.g., sulfate, ammonium, and nitrate by designing a series of sensitivity simulation scenarios. The results show that the estimated emissions of inorganic components over mainland China are increased about five times after including inorganic condensable particulate matter, for both 2014 and 2017. Specifically, taking into account the inorganic condensable particulate matter, increased the average concentrations of sulfate by 104%, ammonium by 10%, nitrate by 11%, and PM<sub>2.5</sub> by 21% for the Hangzhou site in December 2017. Similarly, the simulated average daily concentrations of sulfate from December 3 to 31, 2017, more than doubled, increasing from 3.17 to 8.41  $\mu\text{g m}^{-3}$  for Gucheng, 7.70 to 16.75  $\mu\text{g m}^{-3}$  for Chengdu, 4.08 to 9.43  $\mu\text{g m}^{-3}$  for Lin'an, and 3.19 to 7.22  $\mu\text{g m}^{-3}$  for Dalian.

**Keywords** Condensable particulate matter · Inorganic aerosol · PM<sub>2.5</sub> · Emission · Contribution · Simulated concentration

## Introduction

Despite the improvements in PM<sub>2.5</sub>, i.e., particulate matter with an aerodynamic diameter not exceeding 2.5  $\mu\text{m}$  pollution due to the implementation of emission control policies from 2013 to 2017 by the Chinese government, the annual average mass concentrations of PM<sub>2.5</sub> still exceed the Chinese National Ambient Air Quality Standards (35  $\mu\text{g m}^{-3}$ ) in some megacities with high levels of sulfate ( $\text{SO}_4^{2-}$ ) and ammonium ( $\text{NH}_4^+$ ) and gradually increased nitrate ( $\text{NO}_3^-$ ) concentrations (Tao et al. 2017). The major inorganic compositions in PM<sub>2.5</sub> are  $\text{SO}_4^{2-}$ ,  $\text{NH}_4^+$ , and  $\text{NO}_3^-$ , accounting for 30–50%, and they play an important role in aggravating haze pollution (Reff et al. 2009; Wang et al. 2019). Due to a greater reduction of  $\text{SO}_2$  than  $\text{NO}_x$  (Liu et al. 2019; Zhai et al. 2021), the transition from

sulfate-dominated to nitrate-dominated PM<sub>2.5</sub> pollution has been observed during haze episodes (Xie et al. 2022). There is a large gap between simulated and observed inorganic ion concentrations, attributed to the missing formation mechanisms of secondary inorganic aerosols in air quality models, including reactive nitrogen chemistry in aerosol water, heterogeneous sulfate and nitrate production reactions, and aqueous phase processes (Chen et al. 2016; Cheng et al. 2016; Gao et al. 2021; Shao et al. 2019). The adequate capture of observed peak concentrations is still challenging for regional transport models.

Stationary combustion sources are an important emission source of particulate matter. Total particulate matter includes filterable and condensable particulate matter. Filterable particulate matter exists in solid or liquid phases, while condensable particulate matter is in gas phase in flue but condenses to solid or liquid state by dilution and cooling after discharge into the ambient air (Feng et al. 2018).

Condensable particulate matter contains organic and inorganic fractions, and its species composition is similar to that of submicron and ultrafine filterable particulate matter (Feng et al. 2018). Recently, a number of studies have focused on condensable particulate matter and found that its emissions were much greater than that of filterable particulate matter which have been effectively controlled by ultralow emission standards, lower than  $10 \text{ mg Nm}^{-3}$  (Cano et al. 2017; Li et al. 2017). Considering large emissions of condensable particulate matter, it is necessary to explore their effects on atmospheric  $\text{PM}_{2.5}$ .

Our previous study explored the contributions of organic condensable particulate matter to organic aerosols and  $\text{PM}_{2.5}$  in China (Li et al. 2022). However, few studies used models to explore the contributions of inorganic condensable particulate matter to  $\text{PM}_{2.5}$  and its inorganic components. The inorganic condensable particulate matter mainly consisted of water-soluble ions, e.g.,  $\text{SO}_4^{2-}$ , chloride ( $\text{Cl}^-$ ),  $\text{NH}_4^+$ , and  $\text{NO}_3^-$ , formed through the condensation of gaseous substances, e.g., sulfur trioxide ( $\text{SO}_3$ ), hydrogen chloride ( $\text{HCl}$ ), ammonia ( $\text{NH}_3$ ), and gaseous nitric acid ( $\text{HNO}_3$ ). Measurement results suggested non-negligible emissions of inorganic condensable particulate matter, even accounting for 50% to total condensable particulate matter (Li et al. 2017; Wu et al. 2020). These condensable inorganic fractions may contribute to the formation of water-soluble inorganic ions in  $\text{PM}_{2.5}$  (Wang et al. 2020). A recent study constructed a unit-based condensable particulate matter emission inventory for industrial sources in China, but lacked an assessment of its contributions to  $\text{PM}_{2.5}$  components (Wang et al. 2022). Since the current emission inventory did not involve inorganic condensable particulate matter, the effects of particulate matter emitted from stationary combustion sources on  $\text{PM}_{2.5}$  were underestimated. This study incorporated inorganic condensable particulate matter into the emission inventory and quantify their effects on atmospheric aerosols.

## Experimental

### Estimation of inorganic condensable particulate matter emissions

The method for estimating inorganic condensable particulate matter emissions can refer to the estimation of organic condensable particulate matter emissions, as detailed in Li et al. (2022). The relevant emission information is summarized in Table S1. Totally, 15 stationary combustion source categories were identified. The concentration ratios of total water-soluble inorganic ions in condensable particulate matter to filterable  $\text{PM}_{2.5}$  and percentages of inorganic ionic components, e.g.,  $\text{SO}_4^{2-}$ ,  $\text{Cl}^-$ ,  $\text{NO}_3^-$ ,  $\text{NH}_4^+$ ,  $\text{Na}^+$ ,  $\text{K}^+$ ,  $\text{Mg}^{2+}$ , and  $\text{Ca}^{2+}$ , for these emission sources were calculated as follows in Eqs. (1) and (2), with the results shown in Table S2.

$$\begin{aligned} E_{\text{TWSI}}(\text{CPM}) &= \sum \left[ E_{\text{PM}_{2.5}}(\text{FPM}) \times \frac{E_{\text{TWSI}}(\text{CPM})}{E_{\text{PM}_{2.5}}(\text{FPM})} \right] \\ &= \sum \left[ E_{\text{PM}_{2.5}}(\text{FPM}) \times \frac{C_{\text{TWSI}}(\text{CPM})}{C_{\text{PM}_{2.5}}(\text{FPM})} \right] \end{aligned} \quad (1)$$

$$E_{\text{ions}}(\text{CPM}) = E_{\text{TWSI}}(\text{CPM}) \times \text{Perc\_ion} \quad (2)$$

$E_{\text{TWSI}}(\text{CPM})$  denotes the emission rate of total water-soluble inorganic ions in condensable particulate matter;  $E_{\text{PM}_{2.5}}(\text{FPM})$  denotes the emission rate of filterable  $\text{PM}_{2.5}$ ;  $C_{\text{TWSI}}(\text{CPM})$  denotes the concentration of total water-soluble inorganic ions detected in condensable particulate matter;  $C_{\text{PM}_{2.5}}(\text{FPM})$  denotes the detected concentration of filterable  $\text{PM}_{2.5}$ ;  $E_{\text{ions}}(\text{CPM})$  denotes the emission rate of each inorganic ionic component; and  $\text{Perc\_ion}$  denotes the percentage of each ionic component. Among these parameters, the ratio of  $C_{\text{TWSI}}(\text{CPM})/C_{\text{PM}_{2.5}}(\text{FPM})$  was acquired from the emission survey data.  $E_{\text{PM}_{2.5}}(\text{FPM})$  was derived from  $\text{PM}_{2.5}$  emission rates in the currently used gridded anthropogenic emission inventory. To be consistent with the source sectors of the emission inventory, the collected stationary combustion sources were classified and combined to power plants, iron and steel plants, industrial boilers, cement plants, and other industry processes. It was clear that the emission ratios as well as percentage distributions of inorganic ions varied with different source categories and measurement methods. The indirect dilution method usually monitored lower concentrations of condensable particulate matter than the dry impinger method. But a limited number of measurement studies using dilution methods would make results unrepresentative, so this study combined the values measured by these two methods. The bootstrapping and Monte Carlo simulations were conducted to calculate the mean and uncertainty ranges of  $E_{\text{TWSI}}(\text{CPM})/E_{\text{PM}_{2.5}}(\text{FPM})$  for the above source categories. The detailed method description is shown in Text S1.

### Base model settings and simulation scenarios

In this work, the three-dimensional Community Multi-scale Air Quality Model version 5.3.2 (CMAQv5.3.2) modeling system was applied to simulate spatiotemporal variations of chemical species (Yu et al. 2014; Wyatt Appel et al. 2021). The Weather Research and Forecasting version 3.7 (WRFv3.7) model was applied to generate meteorological fields. The gridded anthropogenic emission inventories for China in 2014 and 2017 were provided by Emission Inventory of Air Benefit and Cost and Attainment Assessment System (EI-ABaCAS) (Zheng et al. 2019). The detailed introduction is shown in Text S2. The simulation domain covered eastern and central China (see Fig. 1a). For the base scenario, the simulations

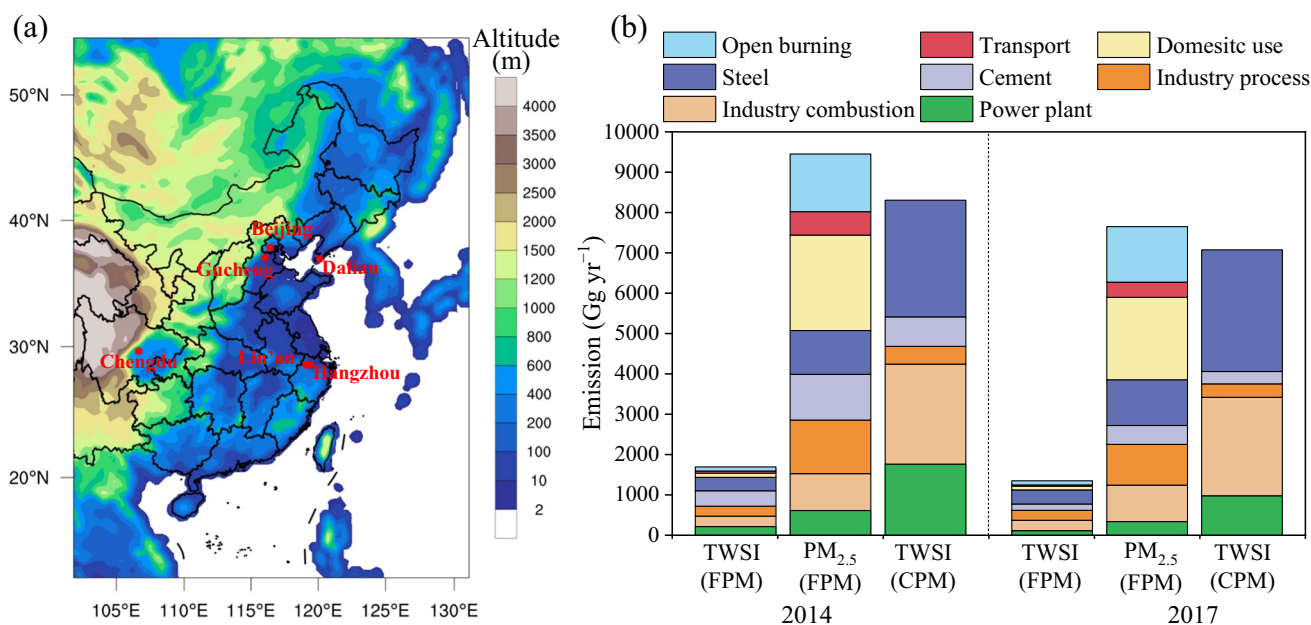
were conducted with the input of previous emission inventory. Then, the estimated emissions of water-soluble inorganic ions in condensable particulate matter were considered as a separate source input into the model. Moreover, on the basis of the estimated uncertainty range, two additional sensitivity cases were performed by reducing the emissions by 41% and enhancing the emissions by 69%. The differences between these sensitivity cases and the base case can indicate the contributions of inorganic condensable particulate matter. Field observations of water-soluble inorganic ions and  $PM_{2.5}$  concentrations at multiple observation sites were used to evaluate model results, as detailed in Text S3.

## Results and discussion

Here, we collected condensable particulate matter (PM) emission information and conducted sensitivity model simulations in order to explore the effects of inorganic condensable particulate matter on atmospheric inorganic aerosols and  $PM_{2.5}$ . The following sections present the estimated emissions of inorganic condensable particulate matter and contributions of condensable particulate matter to inorganic aerosols and  $PM_{2.5}$ .

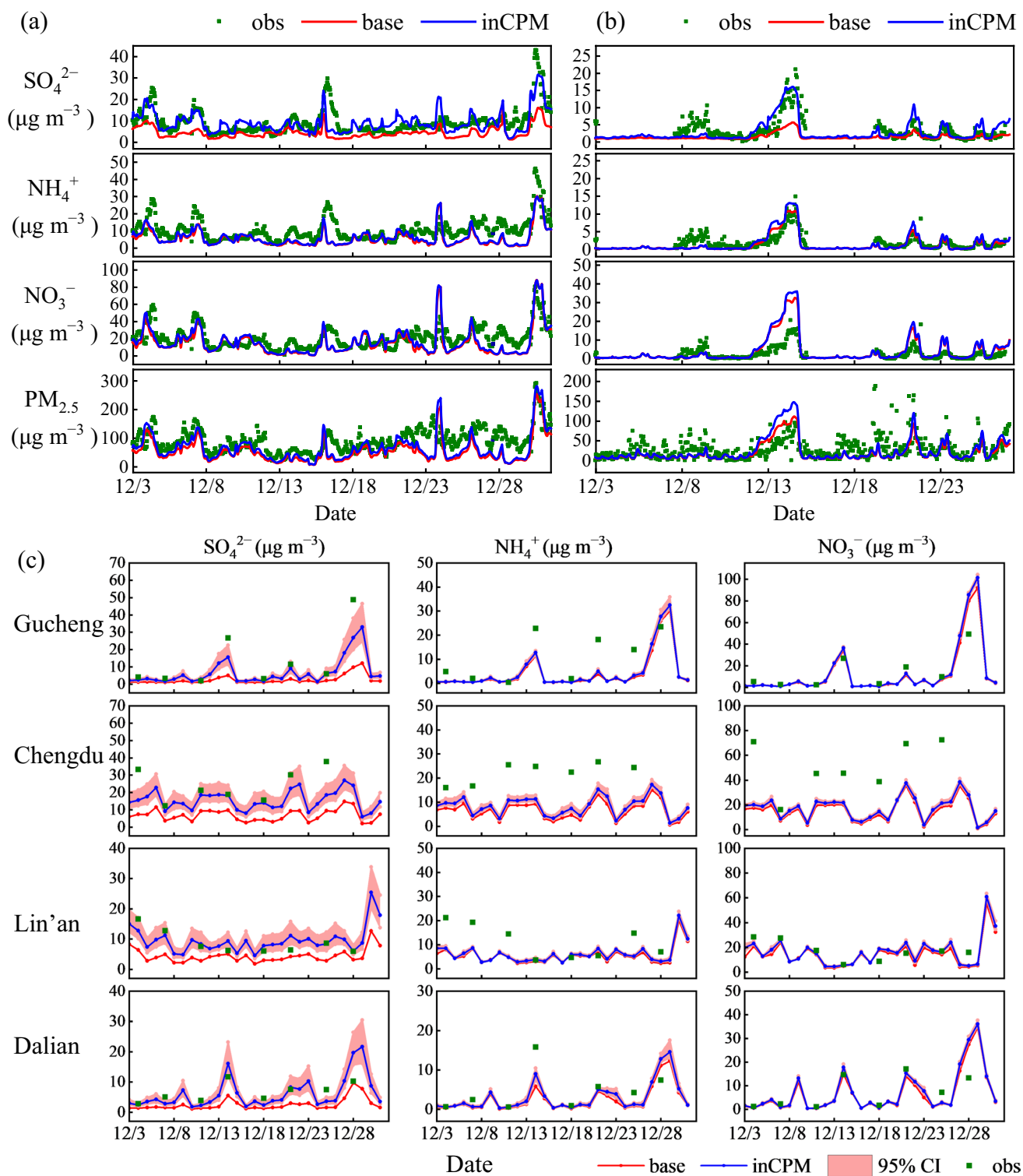
## Emissions of inorganic condensable particulate matter

Figure 1b shows the annual emissions of total water-soluble inorganic ions in filterable particulate matter and condensable particulate matter over China in 2014 and 2017. In the previous emission inventory with only filterable particulate matter, the emissions of inorganic ions both approximately account for 18% of filterable  $PM_{2.5}$  emissions for 2014 and 2017. The estimated emissions of inorganic ions in condensable particulate matter were 8304.9 Gg for 2014 and 7075.0 Gg for 2017, about four times higher than that in filterable  $PM_{2.5}$ . Among the five stationary combustion source sectors, iron and steel plants contributed the most to emissions of inorganic ions, i.e., 35% for 2014 and 43% for 2017, followed by industrial combustion boilers, power plants, cement plants, and other industrial processes. These results suggest that the consideration of inorganic condensable particulate matter greatly increased the emissions of water-soluble inorganic ions and contributions of stationary combustion sources. Then, with regard to the percentage distributions of inorganic ionic components for different source sectors (see Table S4), the most dominant ions were  $SO_4^{2-}$  for power plants, industrial boilers, cement plants, and other industry processes,  $Cl^-$  for iron and steel plants and other industry processes, and  $NH_4^+$  for cement plants.



**Fig. 1** **a** Map of the modeling domain and locations of observational stations. The color shading represents the regional altitude. The names of these stations and their latitude and longitude information are as follows: Beijing (39°58' N, 116°22' E), Gucheng (39°7.8' N, 115°48' E), Dalian (38°54' N, 121°37.8' E), Chengdu (30°39' N, 104°2.4' E), Lin'an (30°18' N, 119°44' E), and Hangzhou (30°18.6' N, 120°4.8' E). **b** Annual emissions of total water-soluble inorganic

ions in filterable particulate matter and condensable particulate matter over China in 2014 and 2017.  $PM_{2.5}$  (FPM) denotes filterable  $PM_{2.5}$ . TWSI (FPM) and TWSI (CPM) denote total water-soluble inorganic ions in filterable and condensable particulate matter, respectively. Note the increases of inorganic ion emissions and contributions of stationary combustion sources after including inorganic condensable particulate matter



**Fig. 2** Observed and simulated hourly concentrations of  $\text{SO}_4^{2-}$ ,  $\text{NH}_4^+$ ,  $\text{NO}_3^-$ , and  $\text{PM}_{2.5}$  before and after including inorganic condensable particulate matter **a** from December 3 to 31, 2017, at the Hangzhou site and **b** from December 3 to 27, 2017, at the Beijing site. **c** Observed and simulated daily concentrations of  $\text{SO}_4^{2-}$ ,  $\text{NH}_4^+$ , and  $\text{NO}_3^-$  during December 3–31, 2017, at Gucheng, Chengdu, Lin'an, and Dalian sites. The base, inCPM, and obs denote base case with

only filterable particulate matter, the case after including inorganic condensable particulate matter, and observation data, respectively. The 95% CI (confidence interval) represents the uncertainty range of inorganic condensable particulate matter contributions caused by uncertainty in emission estimates. Note the improvements of inorganic ion simulations and better capture of observed peaks of  $\text{SO}_4^{2-}$  contributed by inorganic condensable particulate matter

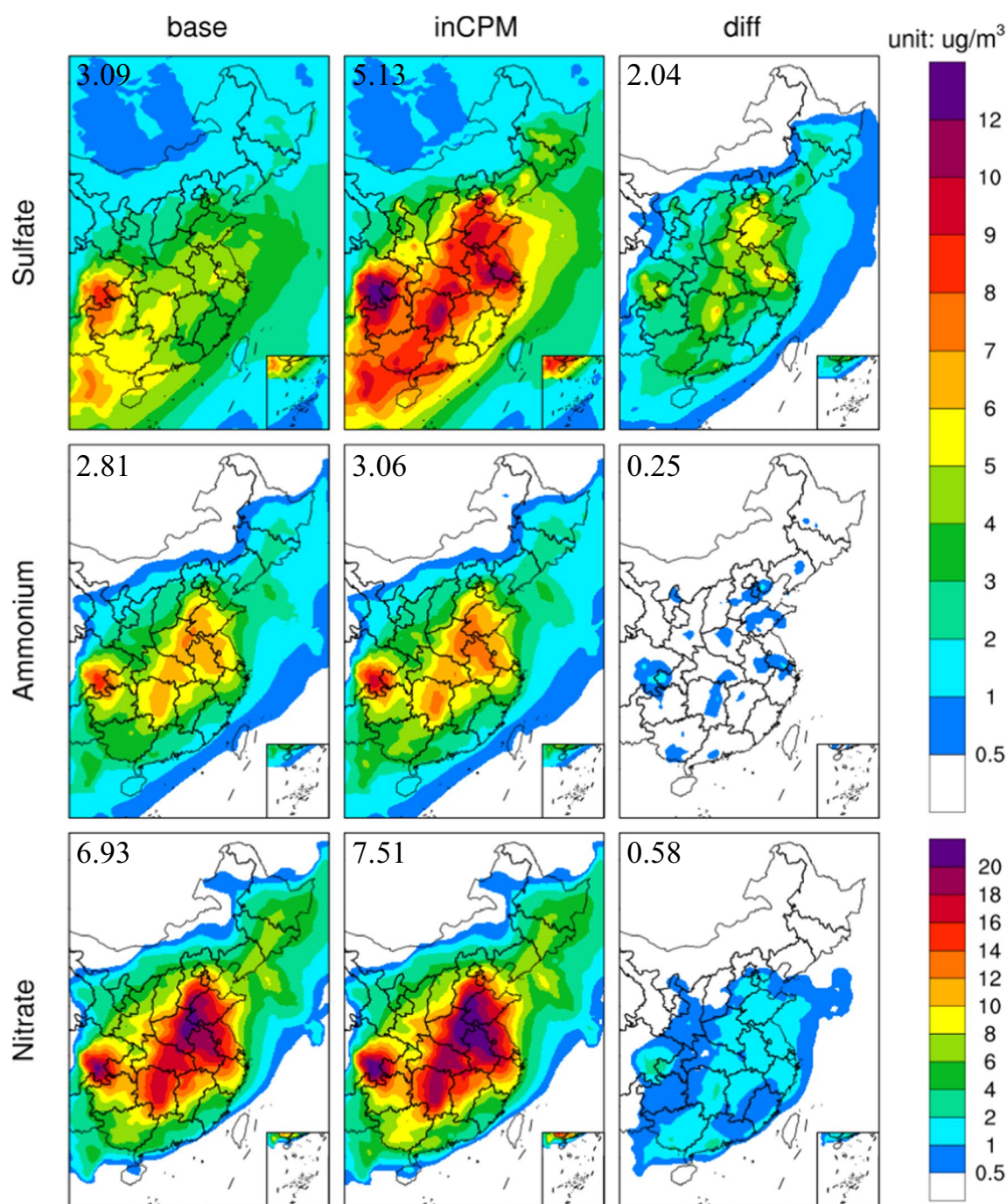


**Fig. 3** Spatial distributions of the average concentrations of sulfate, ammonium, and nitrate during December 3–30, 2017, with only filterable particulate matter (base), with the inclusion of inorganic condensable particulate matter (inCPM), and the difference between

them (diff). The number in the upper left corner of each figure is the value averaged over the study area. Note the varying degrees of improvements of inorganic component concentrations over the study region

### Effects of condensable particulate matter on inorganic aerosols

Concentrations of  $\text{SO}_4^{2-}$ ,  $\text{NH}_4^+$ ,  $\text{NO}_3^-$ , and  $\text{PM}_{2.5}$  in December 2017 were simulated with and without condensable particulate matter, and ground observations for cities in different

regions of China were used to validate the simulation results. The model evaluation results for hourly concentrations of  $\text{SO}_4^{2-}$ ,  $\text{NH}_4^+$ ,  $\text{NO}_3^-$ , and  $\text{PM}_{2.5}$  are shown in Table S5. The improvements in these species after the consideration of condensable particulate matter contributions were observed at these sites from the observed and simulated results. For

the Hangzhou site (see Fig. 2a), the hourly simulations of  $\text{SO}_4^{2-}$  showed large improvements of 0.02–15.64  $\mu\text{g m}^{-3}$ , closing the average gap between simulations and observations from –51.2% to 0.3%. The four observed peaks at 17:00 on December 4, 14:00 on December 7, 13:00 on December 16, and 23:00 on December 30 were better captured. Considering uncertainties in estimated emissions, the contribution ranges of condensable particulate matter to average  $\text{SO}_4^{2-}$ ,  $\text{NH}_4^+$ ,  $\text{NO}_3^-$ , and  $\text{PM}_{2.5}$  concentrations were 2.81–7.95, 0.31–1.14, 1.04–2.69, and 6.77–19.20  $\mu\text{g m}^{-3}$ , respectively. For the Beijing site (see Fig. 2b), the hourly  $\text{SO}_4^{2-}$  concentrations increased by 0.07–11.41  $\mu\text{g m}^{-3}$ , improving the normalized mean bias from –52.6% to 3.6%. The average contribution of condensable particulate matter to  $\text{PM}_{2.5}$  concentrations was 4.51  $\mu\text{g m}^{-3}$ , reducing the underestimation from 28% to 13%.

Figure 2c shows the observed and simulated daily concentrations of  $\text{SO}_4^{2-}$ ,  $\text{NH}_4^+$ , and  $\text{NO}_3^-$  at Gucheng, Chengdu, Lin'an, and Dalian sites. After including condensable particulate matter emissions, the average simulations of  $\text{SO}_4^{2-}$  were improved by 5.25, 9.06, 5.35, and 4.03  $\mu\text{g m}^{-3}$ , respectively. Some high observations were also better captured, such as on December 14 and 28 for Gucheng, December 4 and 7 for Lin'an, and December 14 for Dalian. The estimated contributions of condensable particulate matter to daily  $\text{NH}_4^+$  and  $\text{NO}_3^-$  concentrations were small, with 0.51, 1.87, 0.68, and 0.67  $\mu\text{g m}^{-3}$  to  $\text{NH}_4^+$  and 1.18, 2.23, 2.01, and 0.74  $\mu\text{g m}^{-3}$  to  $\text{NO}_3^-$  for these sites, respectively. To sum up, these results demonstrate that condensable particulate matter was an important source for main inorganic aerosols for cities located in different regions in China.

### Regional contributions of condensable particulate matter to inorganic aerosols and $\text{PM}_{2.5}$

The regional effects of condensable particulate matter on inorganic aerosol and  $\text{PM}_{2.5}$  concentrations averaged over the period of December 3–30, 2017, are shown in Fig. 3. In the base case, the simulated average concentrations of  $\text{SO}_4^{2-}$  and  $\text{NH}_4^+$  over the study region were lower than 9  $\mu\text{g m}^{-3}$ . The  $\text{NO}_3^-$  concentrations were significantly higher than those of  $\text{SO}_4^{2-}$  and  $\text{NH}_4^+$  for most of the study area, consistent with the nitrate-dominated  $\text{PM}_{2.5}$  frequently observed. After including inorganic condensable particulate matter, the simulations of  $\text{SO}_4^{2-}$  for most of the eastern and central regions exceeded 8  $\mu\text{g m}^{-3}$ . The contributions of condensable particulate matter to  $\text{SO}_4^{2-}$  concentrations over most regions varied from 2 to 7  $\mu\text{g m}^{-3}$ . The contributions of condensable particulate matter to  $\text{NH}_4^+$  and  $\text{NO}_3^-$  concentrations were all lower than 3  $\mu\text{g m}^{-3}$ . The  $\text{PM}_{2.5}$  simulations were also improved (see Fig. S4), with contributions varied in the range of 4–20  $\mu\text{g m}^{-3}$  for most areas. Overall, the

$\text{SO}_4^{2-}$ ,  $\text{NH}_4^+$ , and  $\text{NO}_3^-$  simulations over the study region showed varying degrees of improvements, with the largest contribution mainly reflected in  $\text{SO}_4^{2-}$  increases.

## Conclusion

Here, we estimated inorganic condensable particulate matter emissions from stationary combustion sources in China. Results show that the estimated emissions of total water-soluble inorganic ions in condensable particulate matter over mainland China were about four times higher than those in filterable particulate matter for 2014 and 2017. Model results suggest a reasonably better agreement with hourly observations for inorganic ions and  $\text{PM}_{2.5}$  after including inorganic condensable particulate matter for the Hangzhou site in December 2017. The inorganic condensable particulate matter emissions contributed to the average improvements of  $\text{SO}_4^{2-}$ ,  $\text{NH}_4^+$ ,  $\text{NO}_3^-$ , and  $\text{PM}_{2.5}$  concentrations by 4.74, 0.58, 1.66 and 11.38  $\mu\text{g m}^{-3}$ , respectively. Particularly, some underestimated peak observations of  $\text{SO}_4^{2-}$  were better captured. Likewise, the average simulations of  $\text{SO}_4^{2-}$  were improved by 5.25, 9.06, 5.35, and 4.03  $\mu\text{g m}^{-3}$  for Gucheng, Chengdu, Lin'an, and Dalian, respectively. From the perspective of spatial distributions, the simulated concentrations of  $\text{SO}_4^{2-}$ ,  $\text{NH}_4^+$ , and  $\text{NO}_3^-$  over the study region all showed varying degrees of improvements, with the enhancement of  $\text{SO}_4^{2-}$  concentrations much greater than those of  $\text{NH}_4^+$  and  $\text{NO}_3^-$ . This study suggests that condensable particulate matter was a significant emission source and improved the simulation performance of inorganic aerosols and  $\text{PM}_{2.5}$ . Our work stressed the necessity for controlling condensable particulate matter emissions together with filterable particulate matter.

**Supplementary Information** The online version contains supplementary material available at <https://doi.org/10.1007/s10311-023-01644-9>.

**Acknowledgements** The authors would like to thank the comprehensive data collection and sharing platform for atmospheric environmental science as well as the CERN Atmospheric Science Branch of the Institute of Atmospheric Physics, Chinese Academy of Sciences, for providing measurement data of inorganic ions.

**Author contributions** SY and PL conceived and designed the research. ML performed the model simulations. ML conducted data analysis. XC, ZS, WL, XZ, EL, DR, and JHS contributed to the scientific discussions. MZ, YS, ZL, and JJ provided observational data. SY, ML, PL, and JHS wrote and revised the manuscript.

**Funding** This research was supported by the National Natural Science Foundation of China (grant nos. 42175084, 21577126, and 41561144004), the Department of Science and Technology of China (grant nos. 2018YFC0213506 and 2018YFC0213503), and the National Research Program for Key Issues in Air Pollution Control in China (grant no. DQGG0107). Pengfei Li was supported by the

National Natural Science Foundation of China (grant no. 22006030), the Science and Technology Program of Hebei Province (grant no. 22343702D), the Research Foundation of Education Bureau of Hebei (grant no. BJ2020032), and the Initiation Fund of Hebei Agricultural University (grant no. 412201904).

**Data availability** The emission data and model results are available upon request.

## Declarations

**Conflict of interest** The authors declare that they have no conflict of interest.

## References

- Cano M, Vega F, Navarrete B, Plumed A, Camino JA (2017) Characterization of emissions of condensable particulate matter in clinker kilns using a dilution sampling system. *Energy Fuels* 31:7831–7838
- Chen D, Liu Z, Fast J, Ban J (2016) Simulations of sulfate-nitrate-ammonium (SNA) aerosols during the extreme haze events over northern China in October 2014. *Atmos Chem Phys* 16:10707–10724. <https://doi.org/10.5194/acp-16-10707-2016>
- Cheng Y, Zheng G, Wei C, Mu Q, Zheng B, Wang Z, Gao M, Zhang Q, He K, Carmichael G, Pöschl U, Su H (2016) Reactive nitrogen chemistry in aerosol water as a source of sulfate during haze events in China. *Sci Adv* 2:e1601530–e1601530. <https://doi.org/10.1126/sciadv.1601530>
- Feng Y, Li Y, Cui L (2018) Critical review of condensable particulate matter. *Fuel* 224:801–813. <https://doi.org/10.1016/j.fuel.2018.03.118>
- Gao J, Li Y, Li J, Shi G, Liu Z, Han B, Tian X, Wang Y, Feng Y, Russell AG (2021) Impact of formation pathways on secondary inorganic aerosol during haze pollution in Beijing: quantitative evidence from high-resolution observation and modeling. *Geophys Res Lett* 48:1–11. <https://doi.org/10.1029/2021GL095623>
- Li J, Qi Z, Li M, Wu D, Zhou C, Lu S, Yan J, Li X (2017) Physical and chemical characteristics of condensable particulate matter from an ultralow-emission coal-fired power plant. *Energy Fuels* 31:1778–1785. <https://doi.org/10.1021/acs.energyfuels.6b02919>
- Li M, Yu S, Chen X et al (2022) Impacts of condensable particulate matter on atmospheric organic aerosols and fine particulate matter (PM<sub>2.5</sub>) in China. *Atmos Chem Phys* 22:11845–11866. <https://doi.org/10.5194/acp-22-11845-2022>
- Liu M, Huang X, Song Y et al (2019) Ammonia emission control in China would mitigate haze pollution and nitrogen deposition, but worsen acid rain. *Proc Natl Acad Sci* 116:7760–7765. <https://doi.org/10.1073/pnas.1814880116>
- Reff A, Bhawe PV, Simon H, Pace TG, Pouliot GA, Mobley JD, Houyoux M (2009) Emissions inventory of PM<sub>2.5</sub> trace elements across the United States. *Environ Sci Technol* 43:5790–5796. <https://doi.org/10.1021/es802930x>
- Shao J, Chen Q, Wang Y, Lu X, He P, Sun Y, Shah V, Martin RV, Philip S, Song S, Zhao Y, Xie Z, Zhang L, Alexander B (2019) Heterogeneous sulfate aerosol formation mechanisms during wintertime Chinese haze events: air quality model assessment using observations of sulfate oxygen isotopes in Beijing. *Atmos Chem Phys* 19:6107–6123. <https://doi.org/10.5194/acp-19-6107-2019>
- Tao J, Zhang L, Cao J, Zhang R (2017) A review of current knowledge concerning PM<sub>2.5</sub> chemical composition, aerosol optical properties and their relationships across China. *Atmos Chem Phys* 17:9485–9518
- Wang Y, Wang Y, Wang L, Petaja T, Zha Q, Gong C, Li S, Pan Y, Hu B, Xin J, Kulmala M (2019) Increased inorganic aerosol fraction contributes to air pollution and haze in China. *Atmos Chem Phys* 19:5881–5888. <https://doi.org/10.5194/acp-19-5881-2019>
- Wang G, Deng J, Zhang Y, Li Y, Ma Z, Hao J, Jiang J (2020) Evaluating airborne condensable particulate matter measurement methods in typical stationary sources in China. *Environ Sci Technol* 54:1363–1371. <https://doi.org/10.1021/acs.est.9b05282>
- Wang K, Gao J, Liu K, Tong Y, Dan M, Zhang X, Liu C (2022) Unit-based emissions and environmental impacts of industrial condensable particulate matter in China in 2020. *Chemosphere* 303:134759. <https://doi.org/10.1016/j.chemosphere.2022.134759>
- Wu B, Bai X, Liu W, Lin S, Liu S, Luo L, Guo Z, Zhao S, Lv Y, Zhu C, Hao Y LY, Hao J, Duan L, Tian H (2020) Non-negligible stack emissions of noncriteria air pollutants from coal-fired power plants in China: condensable particulate matter and sulfur trioxide. *Environ Sci Technol* 54:6540–6550. <https://doi.org/10.1021/acs.est.0c00297>
- Wyat Appel K, Bash JO, Fahey KM et al (2021) The community multiscale air quality (CMAQ) model versions 5.3 and 5.3.1: system updates and evaluation. *Geosci Model Dev* 14:2867–2897. <https://doi.org/10.5194/gmd-14-2867-2021>
- Xie X, Hu J, Qin M et al (2022) Modeling particulate nitrate in China: current findings and future directions. *Environ Int* 166:107369. <https://doi.org/10.1016/j.envint.2022.107369>
- Yu S, Mathur R, Pleim J et al (2014) Aerosol indirect effect on the grid-scale clouds in the two-way coupled WRF-CMAQ: Model description, development, evaluation and regional analysis. *Atmos Chem Phys* 14:11247–11285. <https://doi.org/10.5194/acp-14-11247-2014>
- Zhai S, Jacob DJ, Wang X et al (2021) Control of particulate nitrate air pollution in China. *Nat Geosci* 14:389–395. <https://doi.org/10.1038/s41561-021-00726-z>
- Zheng H, Cai S, Wang S, Zhao B, Chang X, Hao J (2019) Development of a unit-based industrial emission inventory in the Beijing-Tianjin-Hebei region and resulting improvement in air quality modeling. *Atmos Chem Phys* 19:3447–3462. <https://doi.org/10.5194/acp-19-3447-2019>

## Authors and Affiliations

Mengying Li<sup>1,12</sup> · Shaocai Yu<sup>1</sup>  · Pengfei Li<sup>2</sup> · Xue Chen<sup>1</sup> · Zhe Song<sup>1</sup> · Weiping Liu<sup>1</sup> · Xiaoye Zhang<sup>1,3</sup> · Meigen Zhang<sup>4,5,6</sup> · Yele Sun<sup>4,5</sup> · Zirui Liu<sup>4</sup> · Jingkun Jiang<sup>7,8</sup> · Eric Lichtfouse<sup>9</sup>  · Daniel Rosenfeld<sup>10</sup> · John H. Seinfeld<sup>11</sup>

✉ Shaocai Yu  
shaocaiyu@zju.edu.cn

✉ Pengfei Li  
lpf\_zju@163.com  
Eric Lichtfouse  
eric.lichtfouse@icloud.com

<sup>1</sup> Research Center for Air Pollution and Health, Key Laboratory of Environmental Remediation and Ecological Health, Ministry of Education, College of Environment and Resource Sciences, Zhejiang University, Hangzhou 310058, Zhejiang, People's Republic of China

<sup>2</sup> College of Science and Technology, Hebei Agricultural University, Baoding 071000, Hebei, People's Republic of China

<sup>3</sup> Chinese Academy of Meteorological Sciences, China Meteorological Administration, Beijing 100081, People's Republic of China

<sup>4</sup> State Key Laboratory of Atmospheric Boundary Layer Physics and Atmospheric Chemistry (LAPC), Institute of Atmospheric Physics (IAP), Chinese Academy of Sciences (CAS), Beijing 100029, People's Republic of China

<sup>5</sup> College of Earth and Planetary Sciences, University of Chinese Academy of Sciences, Beijing 100049, People's Republic of China

<sup>6</sup> Center for Excellence in Urban Atmospheric Environment, Institute of Urban Environment, Chinese Academy of Sciences, Xiamen, People's Republic of China

<sup>7</sup> State Key Joint Laboratory of Environment Simulation and Pollution Control, School of Environment, Tsinghua University, Beijing 100084, People's Republic of China

<sup>8</sup> State Environmental Protection Key Laboratory of Sources and Control of Air Pollution Complex, Beijing 100084, People's Republic of China

<sup>9</sup> State Key Laboratory of Multiphase Flow in Power Engineering, Xi'an Jiaotong University, Xi'an, Shaanxi 710049, People's Republic of China

<sup>10</sup> Institute of Earth Sciences, The Hebrew University of Jerusalem, 91904 Jerusalem, Israel

<sup>11</sup> Division of Chemistry and Chemical Engineering, California Institute of Technology, Pasadena, CA 91125, USA

<sup>12</sup> Ecological Civilization Construction Office, Huzhou Municipal Party Committee, Huzhou 313000, Zhejiang, People's Republic of China

### Text S1

For the source categories including power plants, iron and steel plants and industrial boilers, the optimal probability distributions were first determined (see Table S3). Secondly, the statistical bootstrap sampling was applied to obtain the mean value and 95% confidence interval for each source category, with the results of 2.88 (1.84, 4.30), 2.66 (0.75, 8.36), and 2.71 (0.96, 6.46) for power plants, iron and steel plants and industrial boilers, respectively. Thirdly, the total uncertainty range (95% confidence level) was calculated by running 10000 Monte Carlo simulations, which was -41% to 69%. However, the estimated uncertainty ranges were only relevant to variability in  $E_{\text{TWSI}}(\text{CPM})/E_{\text{PM}_{2.5}}(\text{FPM})$  with different emission sources and measurement methods, and it did not necessarily represent the overall emission uncertainty of total water-soluble inorganic ions in condensable particulate matter. A limited number of cement plants and other industrial processes from these emission surveys of inorganic condensable particulate matter cannot support the bootstrapping simulation, thus the calculated values of  $E_{\text{TWSI}}(\text{CPM})/E_{\text{PM}_{2.5}}(\text{FPM})$  for cement plant (0.65) and glass plant (0.33) (see Table S2) were applied to these two source categories, respectively. The percentage distributions of inorganic ionic components were calculated by averaging the percentages of each ion available from multiple sources in these emission surveys, as summarized in Table S4.

### Text S2

CMAQv5.3.2 was the most up-to-date release in July 2021, which contained the updated Carbon Bond gas-phase chemical mechanism 6 (CB6) and a new seventh-generation aerosol module (AERO7). The meteorological inputs of initial and boundary conditions for Weather Research and Forecasting simulations were derived from the National Centers for Environmental Prediction Final Analysis reanalysis dataset with a temporal resolution of 6 h and spatial resolution of  $1^\circ \times 1^\circ$ . The reliability of the Weather Research and Forecasting model has been verified in our previous modeling studies (Wang et al. 2021; Zhang et al. 2021). Anthropogenic emissions from other Asian countries were based on the Emissions Database for Global Atmospheric Research (EDGAR): HTAP v2 ( $0.1^\circ \times 0.1^\circ$ ). Biogenic emissions were calculated online on the basis of Biogenic Emission Inventory System (Carlton and Baker 2011). Dust and sea salt emissions were calculated by an on-line windblown dust scheme (Choi and Fernando 2008) and the sea-salt aerosol algorithms (Gong 2003). For the years 2014 and 2017, the simulation periods were from 25 November to 31 December 2017 and from 22 October to 14 November 2014, with the first 5 days for model spin-up to minimize the effects of initial conditions, respectively.

To define particle size distributions in the CMAQ model, three modes were applied to represent particulate matter, including Aitken with particle size between 0.01 and 0.1  $\mu\text{m}$  formed by nucleation of gas-phase precursors, accumulation with particle size between 0.1 and 1.0  $\mu\text{m}$  formed by the growth of much smaller particles, and coarse with particle size between 2.5 and 10  $\mu\text{m}$ . The modeling parameters used to distribute total emissions to three size categories contained the weight fraction of each mode, the mode geometric mean diameter, and the standard deviation representing lognormal distribution of each aerosol mode (Binkowski and Roselle 2003; Murphy et al. 2021). By default, the weight fraction distribution of Aitken (0.1) and accumulation (0.9) was applied to fine-mode particles.

### Text S3

The hourly inorganic ion observations from 3 to 31 December 2017 located in Zijingang Campus of Zhejiang University in Hangzhou, China ( $30^\circ 18.6' \text{ N}$ ,  $120^\circ 4.8' \text{ E}$ ) were measured by Monitoring of AeRosols and GAses (MARGA 1S, Applinkon Analytical B. V. Corp.) containing a sampling box and an analytic box with the method of ion chromatography. The hourly concentrations of  $\text{PM}_{2.5}$  were measured using TEOM 1405F-FDMS (Thermo Fisher Scientific, Co., Ltd., Waltham, MA, USA). The detailed method descriptions can be found in (Xiong et al. 2021). For the hourly observations from 3 to 27 December 2017, at the Institute of Atmospheric Physics (IAP), Chinese Academy of Science ( $39^\circ 58' \text{ N}$ ,  $116^\circ 22' \text{ E}$ ) in Beijing, the  $\text{PM}_{2.5}$  mass concentrations were measured by a Filter Dynamic Measurement System, and the concentrations of inorganic ions were measured by an online gas and aerosol collector system combined with ion chromatography, as detailed in Liu et al. (2019). During the episode from 27 October to 14 November 2014 at the IAP station, the hourly field observational data of  $\text{PM}_{2.5}$  and inorganic ions in  $\text{PM}_{10}$  were measured by Xu et al. (2015). The  $\text{PM}_{10}/\text{PM}_{2.5}$  ratio of 0.77 was used to calculate the observed concentrations of components in  $\text{PM}_{2.5}$  (Li et al. 2017b). Moreover, the daily mean concentrations (9:00 a.m. to 9:00 a.m. the next day) of inorganic ionic species in  $\text{PM}_{10}$  in December 2017 at the CMA Atmosphere Watch Network (CAWNET) stations in Gucheng ( $39^\circ 7.8' \text{ N}$ ,  $115^\circ 48' \text{ E}$ ), Chengdu ( $30^\circ 39' \text{ N}$ ,  $104^\circ 2.4' \text{ E}$ ), LinAn ( $30^\circ 18' \text{ N}$ ,  $119^\circ 44' \text{ E}$ ) and Dalian ( $38^\circ 54' \text{ N}$ ,  $121^\circ 37.8' \text{ E}$ ) were measured every three days by the Chinese Meteorological Administration using ion chromatography (Dionex 600 series) (Zhang et al. 2012). These cities are

located in different regions in China, including Beijing-Tianjin-Hebei, Chengdu-Chongqing area, Yangtze River Delta and Northeast China, and the regional division map can refer to Wang et al. (2021). Because the inorganic ions were measured in PM<sub>10</sub>, a factor of 0.9 was used to calculate the observed concentrations of these ionic species in PM<sub>2.5</sub>. As for the spatial distributions, the PM<sub>2.5</sub> observations at 1488 national monitoring stations over our modeling domain were collected from the Chinese National Environmental Monitoring Center (CNEMC).

#### **Text S4**

In 2014, the inorganic condensable particulate matter emissions from stationary combustion sources contributed to the improvements of average SO<sub>4</sub><sup>2-</sup>, NH<sub>4</sub><sup>+</sup>, NO<sub>3</sub><sup>-</sup> and PM<sub>2.5</sub> concentrations by 3.57, 0.66, 2.41 and 9.86 μg m<sup>-3</sup>, respectively. The observed peaks on 31 October were well captured after including inorganic condensable particulate matter. However, the simulated concentrations of SO<sub>4</sub><sup>2-</sup>, NH<sub>4</sub><sup>+</sup>, and NO<sub>3</sub><sup>-</sup> were still underestimated on 14 November, which was probably caused by the underestimation of our estimated inorganic condensable particulate matter emissions, the effects of meteorological conditions, or model biases in chemical reactions or gas-particle partition for these inorganic sulfate, ammonium, and nitrate formation.

For Gucheng, there were two observed peaks with the concentrations of 26.76 μg m<sup>-3</sup> on December 14 and 48.85 μg m<sup>-3</sup> on December 28, the simulations were both greatly underestimated by 80% in the base case. After considering inorganic condensable particulate matter emissions, the increases in SO<sub>4</sub><sup>2-</sup> concentrations compared to the base case reached 10.53 and 17.18 μg m<sup>-3</sup>, with the underestimation reduced to 41 and 45%, respectively. When considering the uncertainty ranges of inorganic condensable particulate matter contributions, the increases in SO<sub>4</sub><sup>2-</sup> concentrations ranged from 6.32 to 17.30 on December 14 and from 10.23 to 28.46 μg m<sup>-3</sup> on December 28, among which the maximum emission scenario even resolved 84% and 78% observations, respectively. For Chengdu, some SO<sub>4</sub><sup>2-</sup> observations, such as on December 7, 11, 14, 18, and 21, can be effectively captured after including inorganic condensable particulate matter, with the simulations improved by 5.62 (3.30–9.52), 9.14 (5.36–15.51), 8.55 (5.06–14.36), 9.74 (5.79–16.41), and 13.08 (7.74–22.04) μg m<sup>-3</sup>, respectively. However, the two maximum observations on December 4 and 25 which were both over 30 μg m<sup>-3</sup> were still underestimated, and this can be attributed to uncertainties in our estimated condensable particulate matter emissions, or other missing SO<sub>4</sub><sup>2-</sup> formation mechanisms. For Lin'an and Dalian, the daily SO<sub>4</sub><sup>2-</sup> observations were lower than those in other cities during this study period, and our estimated inorganic condensable particulate matter emissions caused an overestimation for these low observations. Nevertheless, some relatively higher observations, such as on December 4 and 7 in Lin'an, and December 14 in Dalian, were well captured by including condensable particulate matter emission.

Notably, our estimates of inorganic condensable particulate matter emissions from stationary combustion sources contained uncertainties. Due to the lack of extensive measurement data of condensable particulate matter emissions from different sources and regions over China, our construction of the inorganic condensable particulate matter emission inventory in the present study was based on the ratios of  $E_{\text{TWSI}}(\text{CPM})$  to  $E_{\text{PM}_{2.5}}(\text{FPM})$  and the percentage distributions of inorganic ionic components derived from limited source categories.

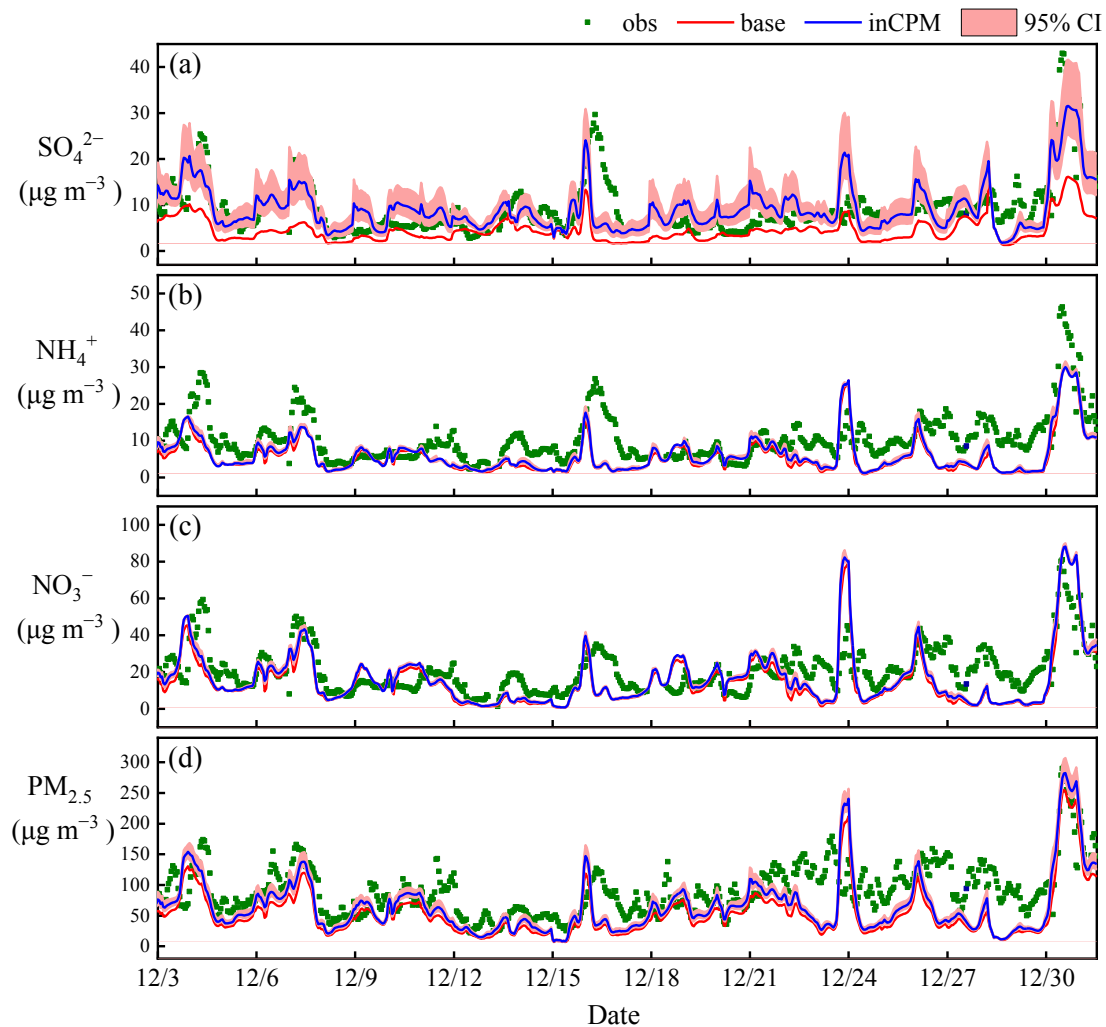


Fig. S1 The observed and simulated hourly concentrations of  $\text{SO}_4^{2-}$ ,  $\text{NH}_4^+$ ,  $\text{NO}_3^-$ , and  $\text{PM}_{2.5}$  during the episode from December 3 to 31, 2017 at the Hangzhou site before and after including inorganic condensable particulate matter emissions. The 95% confidence interval (95% CI) represents the uncertainty range of inorganic CPM contributions caused by uncertainty in emission estimates.

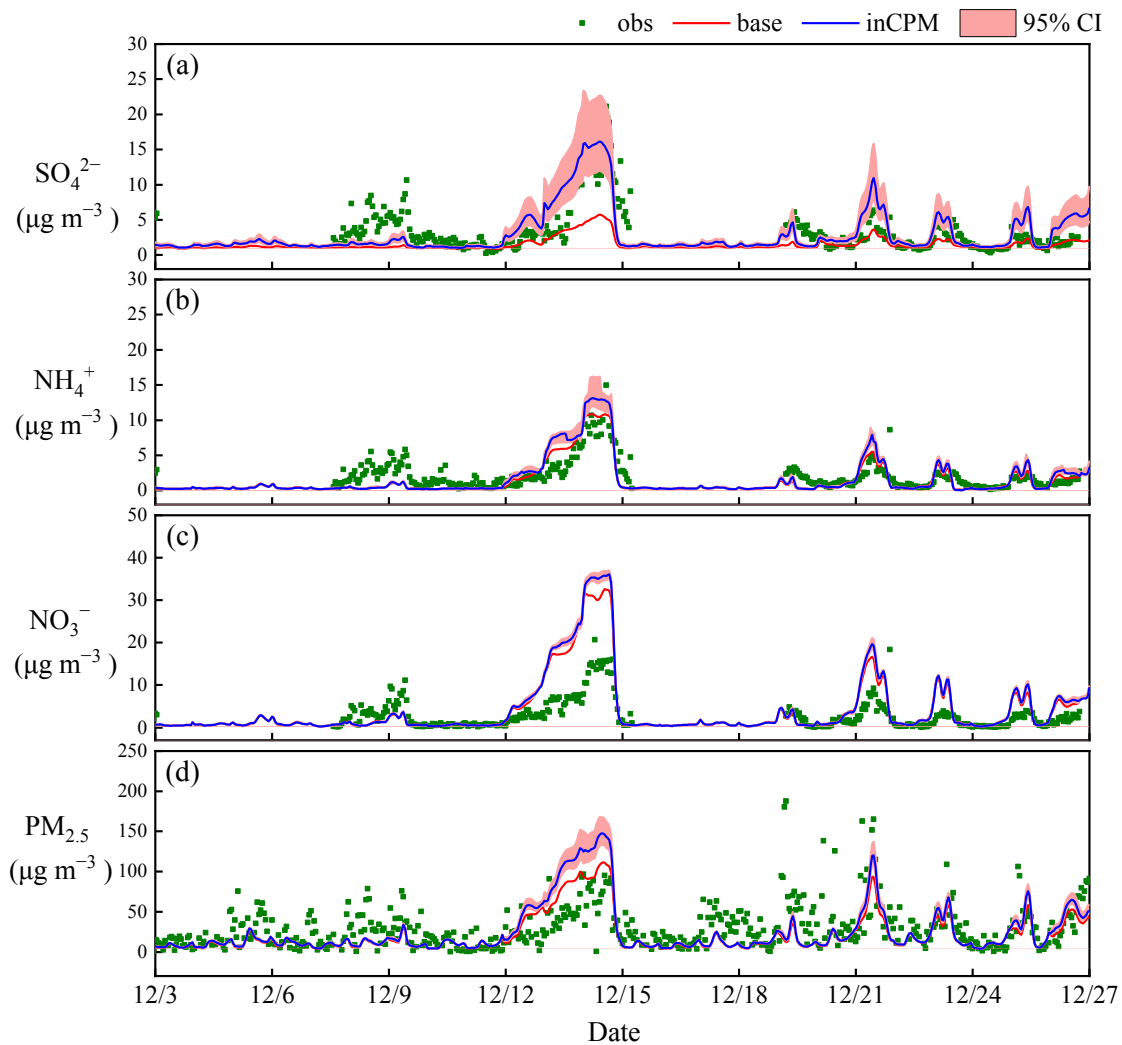


Fig. S2 The observed and simulated hourly concentrations of  $\text{SO}_4^{2-}$ ,  $\text{NH}_4^+$ ,  $\text{NO}_3^-$ , and  $\text{PM}_{2.5}$  during the episode from December 3 to 27, 2017 at the Beijing site before and after including inorganic condensable particulate matter emissions. The 95% confidence interval (95% CI) represents the uncertainty range of inorganic condensable particulate matter contributions caused by uncertainty in emission estimates.

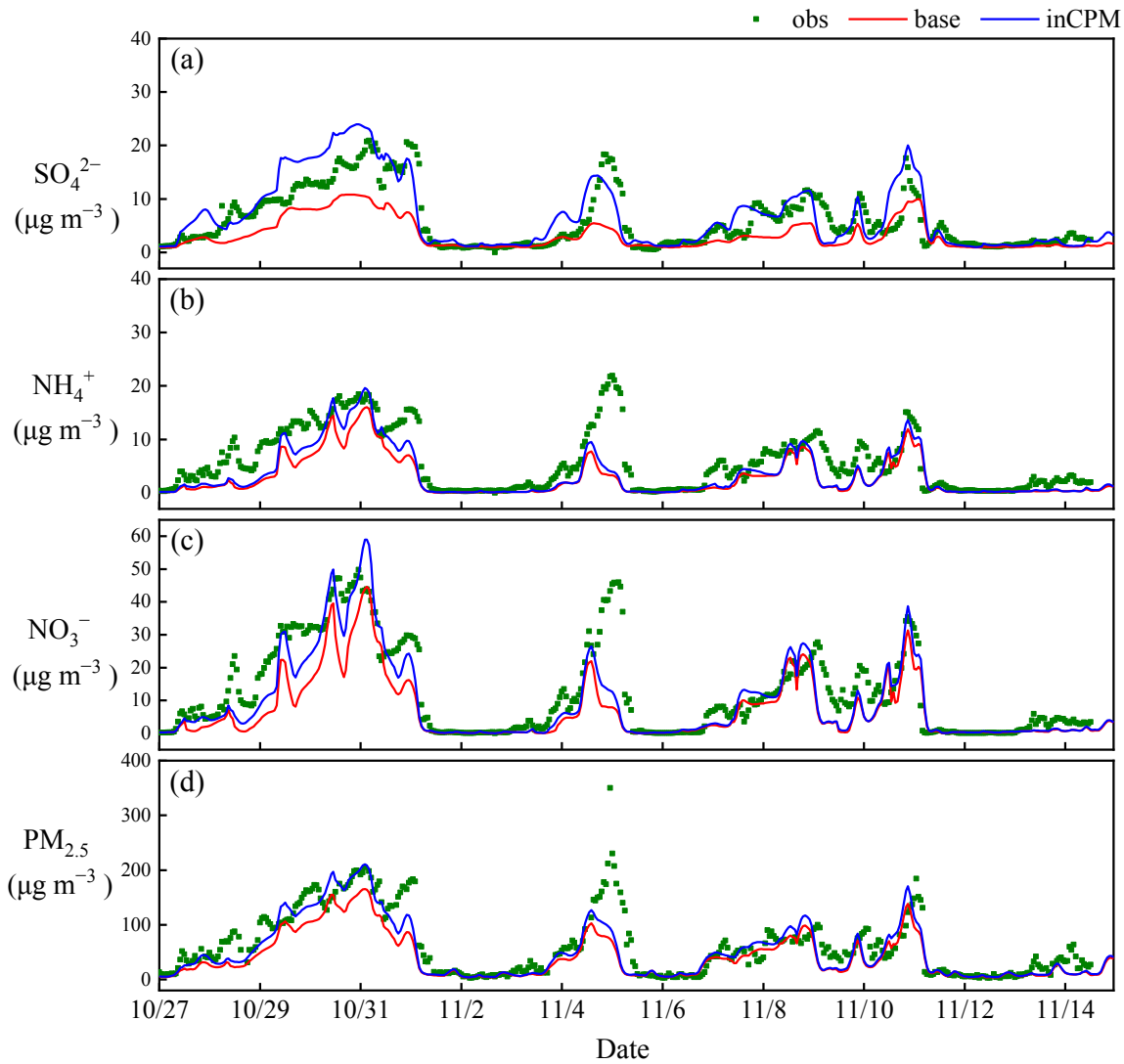


Fig. S3 The observed and simulated hourly concentrations of  $\text{SO}_4^{2-}$ ,  $\text{NH}_4^+$ ,  $\text{NO}_3^-$ , and  $\text{PM}_{2.5}$  during the episode from October 27 to November 14, 2014 at the Beijing site before and after including inorganic condensable particulate matter emissions.

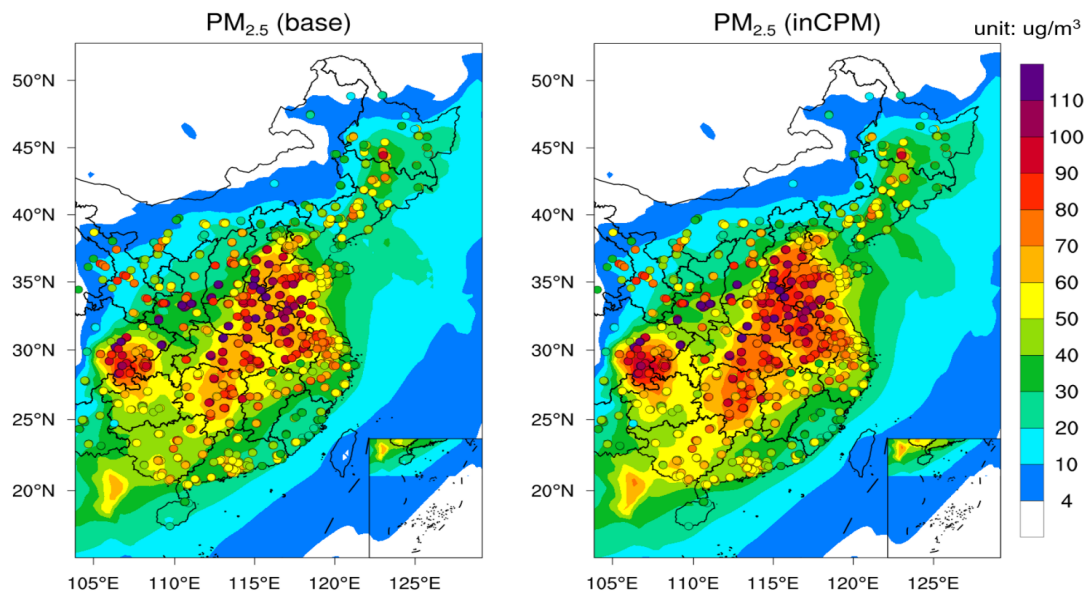


Fig. S4 Spatial distributions of the average PM<sub>2.5</sub> concentrations during December 3–30, 2017 with only filterable particulate matter (base) and with the inclusion of inorganic condensable particulate matter (inCPM). The colored dots denote the observation values for different stations.

Table S1 Existing researches on inorganic condensable particulate matter (CPM) and filterable PM<sub>2.5</sub> (FPM<sub>2.5</sub>) emissions.

Emission sources	Fuel	APCD*	FPM <sub>2.5</sub> (mg/Nm <sup>3</sup> )	CPM (mg/Nm <sup>3</sup> )	CPM-inorganic ions (mg/Nm <sup>3</sup> )					Flue gas volume flow rate	Measurement Methods	References
					TWSI	SO <sub>4</sub> <sup>2-</sup>	Cl <sup>-</sup>	NO <sub>3</sub> <sup>-</sup>	NH <sub>4</sub> <sup>+</sup>			
power plant	coal	SCR+ESP+FF+WFGD	1.04	12.94	6.63						EPA Method 202/ ion chromatography	(Hu et al. 2016)
heating boiler	coal	WFGD	27.41	22.60	7.84							
	coal	FF+WFGD	9.29	22.55	3.84							
industrial boiler	coal	WFGD	46.58	35.81	18.55							
power plant	coal	LNB+SCR+ESP+FF+WFGD	0.98 ±0.17 1.06 ±0.53	TPM 8.23±3.36 7.69±1.68	2.88 3.59	0.707 1.036	0.148 0.268				direct condensation/ ion chromatography	(Hu et al. 2021)
heating boiler	coal	SCR+ FF+WFGD	1.15 ±0.08	4.2 ±1.3	1.3	0.725	0.029	0.161	0.183			
gas power plant	gas	LNB+SCR	0.14 ±0.09	1.99±0.79	1.36	0.375			0.909			
iron and steel coking plant	coal	DFGD +FF+SCR	0.3 0.4 mg/kg	1.2 1.7 mg/kg	0.525					231406 m <sup>3</sup> /h 168.6 t(coal)/ h	indirect dilution ion chromatography	(Zhang et al. 2020)
power plant	coal	SCR+ESP+WFGD+WESP	0.5	7.5/5.8/3.5		3.084 0.118 0.039	0.17 0.000 0.018	0.622 0.000 0.012	0.052 0.024 0.014		dry impinger/ indirect dilution/ direct dilution ion chromatograph	(Wang et al. 2020a)
power plant	coal	SCR+ESP+WFGD	1.5	3/ 2/ 2.5		0.691 0.065 0.054	0.299 0.045 0.034	0.031 0.008 0.000	0.053 0.000 0.002			
power	coal	SCR+ESP+WFGD+	0.3	5.5/1.5/4		1.767	0.046	0.143	0.020			

plant		WESP				0.000 0.005	0.034 0.005	0.003 0.000	0.029 0.005		y	
power plant	coal	SCR+ESP+WFGD+WESP	1.4	2.5/ 1/ 2.5		0.777 0.210 0.054	0.018 0.000 0.005	0.061 0.000 0.009	0.000 0.000 0.008			
power plant	coal	SCR+ESP+WFGD	1.5	11/ 2.5/ 3		4.164 0.090 0.022	0.632 0.000 0.000	0.096 0.000 0.000	0.029 0.005 0.002			
power plant	coal	SCR+ESP+WFGD+WESP	3.3	10/1.5/1.3		2.862 0.438 0.640	0.244 0.000 0.000	0.059 0.000 0.000	0.013 0.022 0.000			
coking plant		DFGD +FF+SCR	0.1	24.5/1.2/0.5		9.587 0.007 0.003	0.268 0.349 0.081	0.231 0.000 0.000	0.562 0.009 0.005			
sintering plant		ESP+ absorption tower	10.9	10/5/1.5		1.601 0.235 0.000	5.200 2.092 0.039	0.040 0.000 0.007	0.276 0.026 0.015			
waste incineration power plant	household garbage	SNCR+SDFGD+DFGD+ activated carbon adsorption+ FF	0.5 0.4	19/ 0.5 21/ 1.0		0.541 0.018 0.835 0.005	10.458 0.093 14.158 0.125	0.532 0.001 0.510 0.001	1.828 0.053 3.861 0.057		dry impinger/ indirect dilution/	
waste incineration power plant	municipal solid waste	SNCR+ SDFGD+ bag filter	0.87± 0.1 0.68±0.19	19.04±3.67 21.09±3.32	4.229 5.7555	0.541 0.835		0.532 0.510	1.828 3.861	131784 m <sup>3</sup> /h 300 t/d 105427 m <sup>3</sup> /h 300 t/d	EPA Method 202/ ion chromatography	(Wang et al. 2018)
power plant	coal	SNCR&SCR+ESP+FGD+ WESP	1.14	3.75		0.15	0.37		0.2	220 t/h	dilution and condensation/ ion chromatography	(Zheng et al. 2018)
power	coal	SCR+ ESP+ GGH	1.1	7.9		0.122	0.0168	0.001			ISO 23210-	(Li et al.

plant		+WFGD+WESP						2			2009/	2017a)
power plant	coal	SCR+LLT-ESP +WFGD+WESP	3.8	36.3		110 mg/g	70	10			EPA Method 202/ ion chromatograph / ICP-MS	(Qi et al. 2017)
			3.8	31.8		45	40	8				
			10.1	40.8		50	60	5				
power plant	coal	SCR+LLT-ESP +WFGD+WESP	3.5	48.7		12				10		(Li et al. 2019)
			7.8	35.2		11				L/min		
power plant	coal	SCR+LLT-ESP +WFGD+WESP	1.81	10.66		1.25	0.71	0.45		368810 0 Nm <sup>3</sup> /h 360.88 t(coal)/ h		(Song et al. 2020)
power plant	coal	SCR+ LLT-ESP+ WFGD+ WESP	1.4	6.66		2.82	0.09	0.02	0.15			(Zhou 2019)
			0.83	6.69		1.73	0.09	0.02	0.18			
			1.14	8.93		2.81	0.09	0.01	0.18			
			1.77	6.66		3.86	0.08	0.01	0.11			
power plant	coal	SCR + BH + SWFGD	0.45±0.0 1 5.25 g/t(coal)	12.7 ± 1.44 142 g/t(coal)			0.313±0.04 7	0.067 ± 0.036		230000 0 Nm <sup>3</sup> /h 275 t/h	EPA Method 201A/ 202/ ion chromatograph y	(Lu et al. 2019)
food processing plant	coal	SCR + ESP + WFGD	1.9±0.1 20.1 g/t(coal)	28.0 ± 6.32 307 g/t(coal)		10.002±2.55 6			2.354±2.27 5	80000 Nm <sup>3</sup> /h 8 t/h		
sintering	coke	ESP+ denitrification+ de-dioxin	1.01	65.3		0.58	0.161	0.000 8	0.321	468 t flux/h	EPA Method 201A/ 202/ ion chromatograph y	(Yang et al. 2015)
coke making	coke oven gas	NA	0.37	89.7		2.551	0.927	0.175	0.851	159 t coal/h		
blast furnace	mixed gas	BH	0.16	3.84		0.0197	0.216	0.039	0.0084	166t steel/h		
oxygen furnace	natural gas	BH	0.15	1.32		0.0333	0.1	0.023 5	0.0055	15.7t waste steel/h		

electric arc furnace	natural gas	CO convertor + BH	0.28	2.02						144t waste steel/h		
industrial boilers	coal	cyclone+ BH	19.3 ± 2.94	27.2 ± 3.49	7.048 ± 1.419	3.439 ± 0.014					(Yang et al. 2018a)	
	wood	wet scrubber	90.8 ± 40.6	31.4 ± 14.1	3.791 ± 0.486	0.284 ± 0.138						
	heavy oil	NA	28 ± 5.6	163 ± 62.8	30.657 ± 4.29	6.231 ± 2.810						
	diesel	NA	0.273	7.67	2.486 ± 0.265	0.384						
	natural gas	NA	0.352 ± 0.157	7.02 ± 3.1	3.635 ± 0.31	0.674 ± 0.267						
industrial boilers	raw coal	cyclone	18.6±13.7	22.7 ± 5.61						EPA Method 201A/ 202/ ion chromatography	(Yang et al. 2018b)	
industrial boilers	raw coal	EP	3.83±1.05	3.92 ± 1.08								
industrial boilers	raw coal	baghouse	3.51±3.21	8.61 ± 4.03								
power plants	raw coal	EP	0.84±0.18	5.96 ± 2.21								
industrial boilers	heavy oil	no	141±76.1	242 ± 131								
industrial boilers	heavy oil	cyclone	22.6±5.28	84.2 ± 38.1								
industrial boilers	heavy oil	BH	2.31	3.16								
boiler	coal	SCR+ESP+WFGD	1.75±0.15	20.30 ±1.51	3.14	2.33	0.22	0.06	0.20	GB/T 16157-1996/ EPA Method 202/ ion	(Yuan et al. 2021)	
boiler	coal	SCR+ESP+WFGD+WESP	3.0 ±1.99	26.0 ±1.53	5.81	4.42	0.50	0.06	0.53			
sintering plant		AS-WFGD+ESP	65.05 ± 1.73	28.68 ±1.15	6.36	4.51	0.25	0.33	0.90			

incineration plant		FFs+ NID+ absorption Tower	6.27±0.76	6.82 ± 0.55	4.01	1.06	1.49	0.34	1.08		chromatography		
cement plant		FFs+ NID+ absorption tower	5.91±0.72	5.41 ± 1.59	3.87	1.73	0.06	0.16	1.83				
glass plant		SCR+FFs+ NID+ absorption tower	12.54±0.5	8.49 ± 0.76	4.16	1.34	1.43	0.65	0.62				
biomass combustion boiler	biomass	SCR/SNCR+ Ultrasonic Dedusting	1.72±0.74	25.50 ±1.50	5.95	1.05	1.70	1.06	1.59				
industrial boiler	coal	SNCR+EFIP+AFGD+UD	2.36	3.98		0.21	0.12	0.04	0.19	52.5 t/h	ISO 23210/ EPA Method 202/ ion chromatography	(Wu et al. 2021)	
industrial boiler	coal	SNCR+BF+WFGD+WESP	1.37	27.01		0.19	0.18	0.10		130 t/h			

Note: Air pollution control devices (APCDs) include selective catalytic reduction denitration device (SCR), selective noncatalytic reduction (SNCR), electrostatic precipitator (ESP), gas-gas heat exchanger (GGH), tube type gas-gas heat exchanger (MGGH), wet flue gas desulfurization (WFGD), wet electrostatic precipitator (WESP), low-low temperature electrostatic precipitator (LLT-ESP), fabric filters (FF), baghouse (BH), seawater flue gas desulfurization (SWFGD), semi-dry flue gas desulphurization (SDFGD), electrostatic-fabric integrated precipitator (EFIP), ammonia flue gas desulphurization device (AFGD), ultrasonic dedusting (UD), and bag filter (BF).

Table S2 The ratios of  $C_{TWSI}(CPM)$  to  $C_{PM_{2.5}}(FPM)$  and the percentages of inorganic ionic components ( $SO_4^{2-}$ ,  $Cl^-$ ,  $NO_3^-$ ,  $NH_4^+$ ,  $Na^+$ ,  $K^+$ ,  $Mg^{2+}$ ,  $Ca^{2+}$ ) in TWSI (CPM) from different emission sources obtained from current measurement studies.

Emission sources	$C_{TWSI}(CPM)/C_{PM_{2.5}}(FPM)$	$SO_4^{2-}$	$Cl^-$	$NO_3^-$	$NH_4^+$	$Na^+$	$K^+$	$Mg^{2+}$	$Ca^{2+}$	Methods	References
coal-fired power plant	6.38									EPA Method 202	(Hu et al. 2016)
	2.94	25%	5%								(Hu et al. 2021)
	3.39	29%	7%								(Wang et al. 2020a)
	10.53	59%	3%	12%	1%	14%	1%	1%	10%		
	0.95	48%	21%	2%	4%	18%	0%	0%	6%		
	8.15	72%	2%	6%	1%	13%	0%	1%	5%		
	0.83	67%	2%	5%		15%	1%	1%	9%		
	3.50	79%	12%	2%	1%	3%	0%	0%	2%		
	1.21	72%	6%	1%	0%	10%	0%	1%	9%		
	1.54	9%	21%		11%						
	0.13	87%	12%	1%							
	1.61	43%	24%	15%		9%	9%				
	2.46	82%	3%	1%	4%	1%		1%	8%		
	2.87	73%	4%	1%	8%	1%		2%	11%		
	3.26	76%	2%	0%	5%	1%		1%	13%		
	2.69	81%	2%	0%	2%	1%		5%	8%		
	2.61		27%	6%					5%		
	0.33	72%	0%	0%	15%	0%	0%	0%	13%		
	0.14	31%	21%	4%	0%	0%	0%	2%	42%		
	0.38	0%	30%	3%	25%	0%	0%	11%	31%		
0.15	100%	0%	0%	0%	0%	0%	0%	0%			
0.07	91%	0%	0%	5%	0%	0%	0%	4%			
0.14	95%	0%	0%	5%	0%	0%	0%	0%			
indirect dilution										(Wang et al. 2020a)	
gas power plant	9.71	28%			67%					EPA Method 202	(Hu et al. 2021)
waste incineration power plant	4.86	13%		13%	43%	18%	2%	1%	10%	EPA Method 202	(Wang et al. 2018)
	8.46	15%		9%	67%	7%	0%	0%	2%		
	29.37	4%	71%	4%	12%	5%	1%	0%	3%		
	49.79	4%	71%	3%	19%	2%	0%	0%	1%	indirect dilution	(Wang et al. 2020a)
	0.37	10%	50%	1%	29%	0%	9%	0%	2%		
	0.47	3%	66%	1%	30%	0%	1%	0%	0%		
iron and steel plant	1.09	53%	15%	0%	29%	1%	1%		1%	EPA Method 202	(Yang et al., 2015)
	15.21	45%	16%	3%	15%	6%	12%		2%		
	4.86	3%	28%	5%	1%	39%	23%		1%		
	2.50	9%	27%	6%	1%	37%	19%		1%		
	128.44	75%	2%	2%	4%	4%	12%	1%	0%	indirect dilution	(Wang et al. 2020a)
	0.66	22%	72%	1%	4%	0%	2%	0%	0%		
	5.22	1%	67%	0%	2%	0%	29%	1%	0%		
	0.37	6%	52%	0%	1%	5%	4%	32%	0%		
1.75										(Zhang et al. 2020)	
sintering plant	0.10	71%	4%	5%	14%	1%	1%	2%	1%	EPA Method	(Yuan et al. 2021)

coal-fired heating boiler	0.29									202	(Hu et al. 2016)
	0.41										(Hu et al. 2021)
	1.13	56%	2%	12%	14%						(Hu et al. 2016)
industrial coal-fired boiler	0.40										(Lu et al. 2019)
	6.50	81%			19%						(Wu et al. 2021)
	0.37	24%	14%	5%	22%	12%	9%	1%	13%		(Yuan et al. 2021)
	0.57	24%	23%	13%	0%	22%	10%	1%	2%		(Yuan et al. 2021)
	1.79	74%	7%	2%	6%	8%	0%	1%	2%		(Yang et al. 2018a)
	1.94	76%	9%	1%	9%	2%	0%	1%	3%		(Yang et al. 2018a)
0.37	49%										
wood-fired boiler	0.04	7%									
heavy oil-fired boiler	1.09	20%									
diesel-fired boiler	9.11	15%									
natural gas-fired boiler	10.33	19%									
biomass combustion boiler	3.46	18%	29%	18%	27%	1%	0%	0%	1%	EPA Method 202	(Yuan et al. 2021)
incineration plant	0.64	26%	37%	8%	27%	1%	0%	0%	0%		
glass plant	0.33	32%	34%	16%	15%	0%	0%	0%	1%		
cement plant	0.65	45%	2%	4%	47%	2%	0%	0%	0%		

Table S3 Probabilistic distributions with uncertainty ranges in the ratio of  $E_{TWSI}(CPM)$  to  $E_{PM2.5}(FPM)$  (95% confidence interval) for each emission source category. Para1 denotes the mean of  $\ln(x)$  for lognormal, and the shape parameter for Weibull. Para2 denotes the standard deviation of  $\ln(x)$  for lognormal, and the scale parameter for Weibull. Mean denotes the average of  $E_{TWSI}(CPM)/E_{PM2.5}(FPM)$  derived from the statistical bootstrap simulation. The total uncertainty of emission was calculated by running Monte Carlo simulations. These measurement data were derived from the references listed in Table S2.

Input parameters	Emission sources	Distribution type	Para 1	Para2	Mean	Uncertainty ranges (95% confidence level)
$E_{TWSI}(CPM)$ $/E_{PM2.5}(FPM)$	Power plants	Weibull	0.84	2.61	2.88	(1.84, 4.30)
	Iron and steel plants	lognormal	0.13	1.27	2.66	(0.75, 8.36)
	Industrial boilers	lognormal	-0.01	1.41	2.71	(0.96, 6.46)
Total						(-41%, 69%)

Table S4 The percentage distributions of inorganic ionic components in TWSI (CPM) for power plants, iron and steel plants, industrial boilers, cement plants, and other industry processes. These percentage distribution data were derived from the references listed in Table S2.

Emission sources	$E_{TWSI}(CPM)$ $/E_{PM2.5}(FPM)$	SO <sub>4</sub> <sup>2-</sup>	Cl <sup>-</sup>	NO <sub>3</sub> <sup>-</sup>	NH <sub>4</sub> <sup>+</sup>	Na <sup>+</sup>	K <sup>+</sup>	Mg <sup>2+</sup>	Ca <sup>2+</sup>
Power plants	2.88	52%	13%	4%	15%	5%	1%	1%	9%
Iron and steel plants	2.66	22%	35%	2%	14%	11%	10%	5%	1%
Industrial boilers	2.71	40%	18%	9%	17%	8%	3%	1%	4%
Cement plants	0.65	45%	2%	4%	47%	2%	0%	0%	0%
Other industry processes	0.33	32%	34%	16%	15%	0%	0%	0%	1%

Table S5. Model evaluation statistics for hourly concentrations of  $\text{SO}_4^{2-}$ ,  $\text{NH}_4^+$ ,  $\text{NO}_3^-$ , and  $\text{PM}_{2.5}$  during December 3–31, 2017 in Hangzhou, December 3–27, 2017 and October 27–November 14, 2014 in Beijing. inCPM denotes the case after including inorganic condensable particulate matter. OBS and SIM denote the mean observed and simulated concentrations ( $\mu\text{g m}^{-3}$ ), respectively. N, MB, NMB and R denote number of observations, mean bias, normalized mean bias, and correlation coefficient, respectively.

Period	City	Species	Cases	N	OBS	SIM	MB	NMB	R
December 3–31, 2017	Hangzhou, China	$\text{SO}_4^{2-}$	base	660	9.33	4.56	-4.77	-51.2%	0.65
			inCPM		9.33	9.30	-0.03	-0.3%	0.64
		$\text{NH}_4^+$	base	660	10.57	5.71	-4.86	-46.0%	0.64
			inCPM		10.57	6.29	-4.28	-40.5%	0.64
		$\text{NO}_3^-$	base	666	20.82	15.25	-5.57	-26.8%	0.62
			inCPM		20.82	16.91	-3.91	-18.8%	0.63
		$\text{PM}_{2.5}$	base	679	90.38	54.10	-36.28	-40.1%	0.63
			inCPM		90.38	65.48	-24.90	-27.6%	0.61
December 3–27, 2017	Beijing, China	$\text{SO}_4^{2-}$	base	364	3.56	1.69	-1.87	-52.6%	0.74
			inCPM		3.56	3.69	0.13	3.6%	0.72
		$\text{NH}_4^+$	base	365	2.29	1.84	-0.45	-19.8%	0.61
			inCPM		2.29	2.17	-0.12	-5.3%	0.60
		$\text{NO}_3^-$	base	365	2.92	5.45	2.53	86.6%	0.83
			inCPM		2.92	5.94	3.02	103.5%	0.84
		$\text{PM}_{2.5}$	base	529	30.92	22.36	-8.56	-27.7%	0.50
			inCPM		30.92	26.87	-4.05	-13.1%	0.50
October 27–November 14, 2014	Beijing, China	$\text{SO}_4^{2-}$	base	443	5.90	3.28	-2.62	-44.4%	0.84
			inCPM		5.90	6.85	0.95	16.1%	0.86
		$\text{NH}_4^+$	base	443	5.67	2.82	-2.85	-50.3%	0.80
			inCPM		5.67	3.48	-2.19	-38.6%	0.82
		$\text{NO}_3^-$	base	443	12.23	6.95	-5.28	-43.2%	0.81
			inCPM		12.23	9.36	-2.87	-23.5%	0.85
		$\text{PM}_{2.5}$	base	410	61.22	40.87	-20.35	-33.2%	0.84
			inCPM		61.22	50.73	-10.49	-17.1%	0.85

## References

- Binkowski FS, Roselle SJ (2003) Models-3 Community Multiscale Air Quality (CMAQ) model aerosol component 1. Model description. *J Geophys Res Atmos* 108:4183–n/a. <https://doi.org/10.1029/2001jd001409>
- Carlton AG, Baker KR (2011) Photochemical modeling of the ozark isoprene volcano: MEGAN, BEIS, and their impacts on air quality predictions. *Environ Sci Technol* 45:4438–4445. <https://doi.org/10.1021/es200050x>
- Choi YJ, Fernando HJS (2008) Implementation of a windblown dust parameterization into MODELS-3/CMAQ: Application to episodic PM events in the US/Mexico border. *Atmos Environ* 42:6039–6046. <https://doi.org/10.1016/j.atmosenv.2008.03.038>
- Gong SL (2003) A parameterization of sea-salt aerosol source function for sub- and super-micron particles. *Global Biogeochem Cycles* 17:1–7. <https://doi.org/10.1029/2003gb002079>
- Hu Y, Feng Y, Wang C et al (2016) Studies on monitoring method of condensable particulate and water-soluble ions in fumes from

- coal fired boilers. *Environ Monit Manag Technol* 28(1):41–45. <http://lib.cqvip.com/Qikan/Article/Detail?id=667763259>
- Li J (2018) Experimental study on emission characteristics of condensable particulate matter and typical organic pollutants in coal-fired flue gas. PhD thesis, School of Energy Engineering, Zhejiang University, China, 164 pp., <https://kns.cnki.net/KCMS/detail/detail.aspx?dbname=CDFDLAST2019&filename=1019028601.nh> (last access: 8 December 2022)
- Li J, Qi Z, Li M et al (2017a) Physical and chemical characteristics of condensable particulate matter from an ultralow-emission coal-fired power plant. *Energy and Fuels* 31(2):1778–1785. <https://doi.org/10.1021/acs.energyfuels.6b02919>
- Li J, Zhang M, Wu F et al (2017b) Assessment of the impacts of aromatic VOC emissions and yields of SOA on SOA concentrations with the air quality model RAMS-CMAQ. *Atmos Environ* 158:105–115. <https://doi.org/10.1016/j.atmosenv.2017.03.035>
- Li X, Zhou C, Li J et al (2019) Distribution and emission characteristics of filterable and condensable particulate matter before and after a low-low temperature electrostatic precipitator. *Environ Sci Pollut Res* 26:12798–12806. <https://doi.org/10.1007/s11356-019-04570-y>
- Liu Z, Hu B, Ji D et al (2019b) Characteristics of fine particle explosive growth events in Beijing, China: Seasonal variation, chemical evolution pattern and formation mechanism. *Sci Total Environ* 687:1073–1086. <https://doi.org/10.1016/j.scitotenv.2019.06.068>
- Lu CM, Dat ND, Lien CK et al (2019) Characteristics of fine particulate matter and polycyclic aromatic hydrocarbons emitted from coal combustion processes. *Energy and Fuels* 33(10):10247–10254. <https://doi.org/10.1021/acs.energyfuels.9b02201>
- Murphy BN, Nolte CG, Sidi F et al (2021) The detailed emissions scaling, isolation, and diagnostic (DESID) module in the Community Multiscale Air Quality (CMAQ) modeling system version 5.3.2. *Geosci Model Dev* 14:3407–3420. <https://doi.org/10.5194/gmd-14-3407-2021>
- Pei B (2015) Determination and emission of condensable particulate matter from coal-fired power plants. *Huanjing Kexue* 36(5):1544–1549. <https://doi.org/10.13227/j.hjkk.2015.05.005>
- Qi Z, Li J, Wu D et al (2017) Particulate matter emission characteristics and removal efficiencies of a low-low temperature electrostatic precipitator. *Energy and Fuels* 31(2):1741–1746. <https://doi.org/10.1021/acs.energyfuels.6b02692>
- Song J, Lu S, Wu Y et al (2020) Migration and distribution characteristics of organic and inorganic fractions in condensable particulate matter emitted from an ultralow emission coal-fired power plant. *Chemosphere* 243:125346. <https://doi.org/10.1016/j.chemosphere.2019.125346>
- Wang G, Deng J, Ma Z et al (2018) Characteristics of filterable and condensable particulate matter emitted from two waste incineration power plants in China. *Sci Total Environ* 639:695–704. <https://doi.org/10.1016/j.scitotenv.2018.05.105>
- Wang G, Deng J, Zhang Y et al (2020a) Evaluating airborne condensable particulate matter measurement methods in typical stationary sources in China. *Environ Sci Technol* 54(3):1363–1371. <https://doi.org/10.1021/acs.est.9b05282>
- Wang K, Yang L, Li J et al (2020b) Characteristics of condensable particulate matter before and after wet flue gas desulfurization and wet electrostatic precipitator from ultra-low emission coal-fired power plants in China. *Fuel* 278:118206. <https://doi.org/10.1016/j.fuel.2020.118206>
- Wang L, Chen X, Zhang Y et al (2021) Switching to electric vehicles can lead to significant reductions of PM<sub>2.5</sub> and NO<sub>2</sub> across China. *One Earth* 4:1037–1048. <https://doi.org/10.1016/j.oneear.2021.06.008>
- Wu B, Bai X, Liu W et al (2020) Non-Negligible Stack Emissions of Noncriteria Air Pollutants from Coal-Fired Power Plants in China: Condensable Particulate Matter and Sulfur Trioxide. *Environ Sci Technol* 54(11):6540–6550. <https://doi.org/10.1021/acs.est.0c00297>
- Xiong C, Yu S, Chen X et al (2021) Dominant contributions of secondary aerosols and vehicle emissions to water-soluble inorganic ions of PM<sub>2.5</sub> in an urban site in the metropolitan Hangzhou, China. *Atmosphere* 12. <https://doi.org/10.3390/atmos12111529>
- Xu WQ, Sun YL, Chen C et al (2015) Aerosol composition, oxidation properties, and sources in Beijing: Results from the 2014 Asia-Pacific Economic Cooperation summit study. *Atmos Chem Phys* 15:13681–13698. <https://doi.org/10.5194/acp-15-13681-2015>
- Yang F, Li Z, Liu H et al (2021) Emission characteristics of condensable particulate matter and sulfur trioxide from coal-fired power plants. *J Energy Inst* 94:146–156. <https://doi.org/10.1016/j.joei.2020.12.003>
- Yang HH, Lee KT, Hsieh YS et al (2014) Filterable and condensable fine particulate emissions from stationary sources. *Aerosol*

- Air Qual Res 14:2010–2016. <https://doi.org/10.4209/aaqr.2014.08.0175>
- Yang HH, Lee KT, Hsieh, YS et al (2015) Emission characteristics and chemical compositions of both filterable and condensable fine particulate from steel plants. *Aerosol Air Qual Res* 15(4):1672–1680. <https://doi.org/10.4209/aaqr.2015.06.0398>
- Yang HH, Luo SW, Lee KT et al (2016) Fine particulate speciation profile and emission factor of municipal solid waste incinerator established by dilution sampling method. *J Air Waste Manag Assoc* 66(8):807–814. <https://doi.org/10.1080/10962247.2016.1184195>
- Yang HH, Arafath, SM, Lee KT et al (2018a) Chemical characteristics of filterable and condensable PM<sub>2.5</sub> emissions from industrial boilers with five different fuels. *Fuel* 232(168):415–422. <https://doi.org/10.1016/j.fuel.2018.05.080>.
- Yang HH, Arafath SM, Wang YF et al (2018b) Comparison of coal- and oil-fired boilers through the investigation of filterable and condensable PM<sub>2.5</sub> sample analysis. *Energy and Fuels* 32(3):2993–3002. <https://doi.org/10.1021/acs.energyfuels.7b03541>
- Zhang XY, Wang YQ, Niu T et al (2012) Atmospheric aerosol compositions in China: Spatial/temporal variability, chemical signature, regional haze distribution and comparisons with global aerosols. *Atmos Chem Phys* 12:779–799. <https://doi.org/10.5194/acp-12-779-2012>
- Zhang Y, Chen X, Yu S et al (2021) City-level air quality improvement in the Beijing-Tianjin-Hebei region from 2016/17 to 2017/18 heating seasons: Attributions and process analysis. *Environ Pollut* 274:116523. <https://doi.org/10.1016/j.envpol.2021.116523>
- Zhang Y, Deng J, Wang G et al (2020) Characterization of condensable particulate matter emitted from a typical coking plant in iron and steel plant. *Environ Eng* 38:154–158+125. <https://doi.org/10.13205/j.hjgc.202009025>
- Zheng C, Hong Y, Liu S et al (2018) Removal and emission characteristics of condensable particulate matter in an ultralow emission power plant. *Energy and Fuels* 32(10):10586–10594. <https://doi.org/10.1021/acs.energyfuels.8b02464>
- Zhou C (2019) Experimental study on emission and distribution characteristics of organic pollutants in condensable particulate matter in coal-fired flue gas. Master thesis, School of Energy Engineering, Zhejiang University, China, 82 pp., <https://doi.org/10.27461/d.cnki.gzjdx.2019.001904>